Natural Resources Canada | Ressources naturelles Canada

GEOLOGICAL SURVEY OF CANADA
OPEN FILE 8237

3-D modelling of magnetotelluric data from the western Superior Province, Ontario

E. Roots and J.A. Craven

2017

GEOLOGICAL SURVEY OF CANADA
OPEN FILE 8237

3-D modelling of magnetotelluric data from the western Superior Province, Ontario

E. Roots and J.A. Craven

2017

doi:10.4095/300668

This publication is available for free download through GEOSCAN (http://geoscan.nrcan.gc.ca/).

Recommended citation
Roots, E. and Craven, J.A., 2017. 3-D modelling of magnetotelluric data from the western Superior Province, Ontario; Geological Survey of Canada, Open File 8237, 24 p. doi:10.4095/300668

Publications in this series have not been edited; they are released as submitted by the author.

Introduction

Magnetotelluric geophysical exploration comprises the measurement of time-varying fluctuations of the natural electric and magnetic fields of the Earth (Cagniard, 1953; Tikhonov, 1950). Data from multiple sites spanning a survey area are analyzed in the frequency domain and used to map the spatial variation of the subsurface electrical properties (i.e. the resistivity). In the frequency domain a skin effect controls the depth of investigation and for simple layered earth structure (1-D) signals with longer periods (or lower frequencies) penetrate to deeper layers than shorter periods (or higher frequency) signals. If a broad range of frequencies at each site are measured then the variation of resistivity with depth can be determined.

Enhanced electrical conductivity (the inverse of resistivity) in the crust is often linked to the presence and mobility of charges within a variety of material: aqueous fluids within porous strata (e.g., Glover and Vine, 1995; Hyndman et al., 1993), graphite, interconnected grains of metallic oxides, and sulphides, (e.g., Jones and Craven, 1990; Katsube and Mareschal, 1993; Li et al., 2003). Laboratory studies have indicated there are several sources of enhanced electrical conductivity in the mantle, including graphite, hydrogen, partial melt, water, and temperature variation (e.g., Constable, 2006; Ducea and Park, 2000; Hirth et al., 2000; Jones, 1999; Karato, 1990; Korja, 2007; Selway, 2013; Yoshino et al., 2008). The spatial variation of the resistivity can also be used to infer processes that have led to the formation and subsequent modification of a region (e.g., Evans et al., 2011; Ferguson et al., 2012; Spratt et al., 2009).

The western Superior craton is a Neoarchean tectonic collage (Card, 1990) interpreted to represent terrane accretion (Card, 1990; Percival et al., 2006) and is therefore an important laboratory in which to conduct experiments to test hypothecs of Archean tectonic evolution. The intent of this open file is to publish recent work of legacy MT data (Ferguson et al., 2005) using 3D analysis methods to provide a framework for further MT work in the Superior Province in other programs. As such only a cursory analysis of the major conductive features is discussed herein and a more in depth investigation is left for future work.

Data Selection

Full impedance tensor and transfer function data was collected at 213 sites over an area spanning 936 km west-east and 983 km south-north. Overall, the impedance data is of good quality (relatively low data errors and smoothly varying), while the quality of the transfer function data varies from site to site. The periods available in the dataset range from 0.002 s to 30720 s, however as the dataset is actually a compilation of 5 different datasets collected over 3 years, many of the periods are only available at a fraction of the sites. In particular, data with periods less than 1 second are only available at 25% of the sites. The lack of data at periods < 1 s, combined with the large area covered by the survey effectively restricts the sensible period choices to those greater than 1 s. It should also be noted that while all sites recorded at periods between 4 s and 1280 s, the highest periods were recorded at ~70% of sites. With all of this in mind, 8 periods were selected between 4 and 10000 s (2 periods per decade), ensuring as much as possible that the chosen periods were available at as many sites as possible.

Based on the available computational resources, inversion of all 12 data components at 8 periods for all 213 sites was impossible. However, the fact that only relatively long periods are being inverted allows many of the sites to be removed based on their close proximity to others. In order to estimate optimal site spacing, the MT sensitivity matrix was calculated over a half-space of 10000 Ω-m for a single site at the lowest period to be inverted (4 s). Figure 1 shows the resulting sensitivities at a depth of 3 km. The overlaid contours show where the sensitivities fall off to 10%, 0.1% and 0.0001% of their maximum. The radius of the first contour is ~20 km, which suggests that for periods of 4 s or greater, sites within 20 km of each other likely contain redundant data. Visual inspection of the data in general confirms this. Of the 213 original sites, 92 sites were removed on this basis. An additional 11 sites were removed from the eastern-most portion of the survey in order to optimize the use of mesh in the inversion.

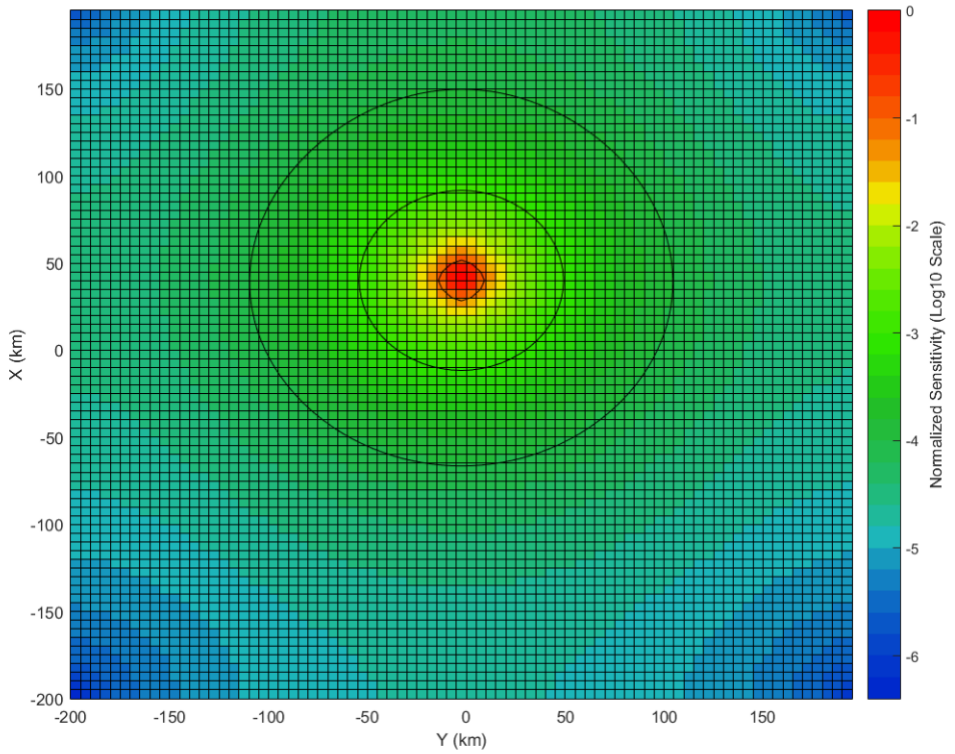

Figure 1: Sensitivity values calculated over a half space of 10000 Ω-m at a depth of 3 km. Contour lines show constant sensitivity values of 10^{-1}, 10^{-3} and 10^{-4}. A mesh with constant spacing (5 km) was used to ensure the choice of mesh did not affect the calculated sensitivities.

3D Modelling Overview

Data was inverted using the WSINV3DMT modelling code (Siripunvaraporn et al., 2005). The code uses the Occam approach which seeks a model with minimum structure and appropriate fit to the provided data. Orienting the mesh and data with geological structure is useful when the diagonal components of the impedance tensor are not being inverted (Kiyan et al., 2014). In order to simplify interpretation, the mesh and data azimuths were set to 0˚, and the diagonal components were included. These components tend to have higher associated errors than the off-diagonal components, and so are typically down-weighted in the inversion process. This down-weighting typically takes the form of increasing the associated errors. If the errors are increased by a large factor (in the past, a factor as high as 300 has been used), the inversion process practically ignores the diagonal components. In order to strike a compromise between being able to match all the data without overfitting to noise, the errors associated with the diagonal components were increased by a factor of 5. Error floors of 7.5% and 20% were applied to the impedance and tipper data, respectively.

Beginning with a half-space model (Figure 2), the inversion was run for 3 iterations. The best fitting model among these was then set as the starting model, and another 3 iterations were run. This process was repeated a total of 5 times, eventually reaching a model whose response fits the data with an RMS of 2.28. The process of restarting the inversion using the previous best-fitting model in general leads to better models with lower RMS than letting a single inversion run for many iterations.

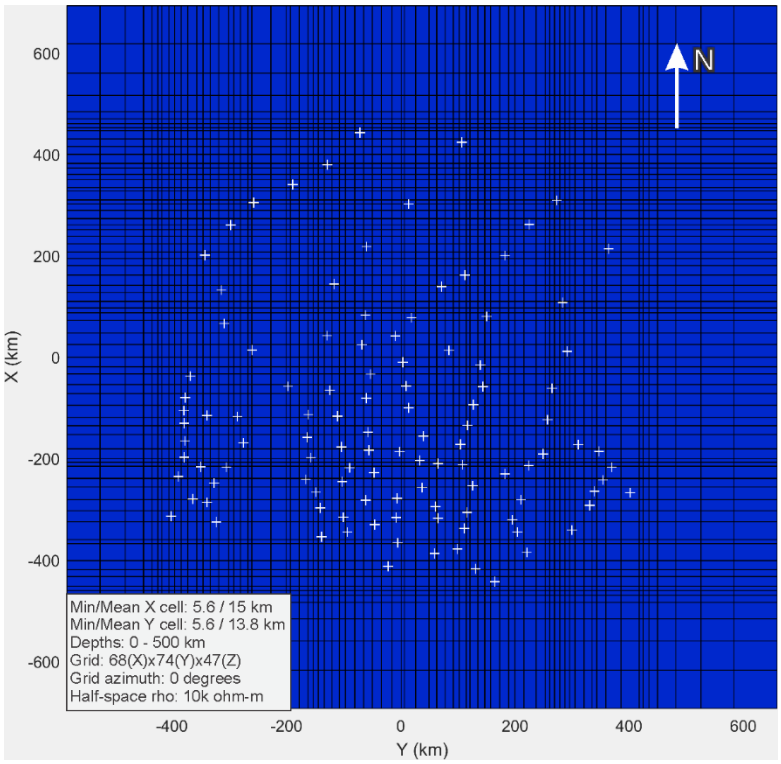

Figure 2: Initial model used for inversion. '+' signs indicate site locations.

Figures 3, 4, and 5 show a collection of depth slices taken throughout the final model. Due to a combination of sparse mesh in the Z direction and the lack of low periods in the inverted data, the features within top 10 km of the model are somewhat sporadic. Below ~3 km depth, the model is largely resistive, particularly to the north of the model, with values ranging from 1000 to 100000 Ω-m. Small localized conductors are scattered throughout southern portion of the model between 5 and 10 km depth. For the periods inverted here, structure seen at depths shallower than 10 km is constrained mostly by the choice of regularization and starting model rather than the data (Bedrosian, 2016), and is unlikely to correspond with real geological structure. The model remains fairly resistive between 10 and 25 km depth within the Northern Caribou (NC) terrane and northward. At these depths, the only noticeably conductive regions (i.e. resistivity < 1000 Ω-m) are to the southeast and southwest. There is

also a region with resistivity values less than 1000 Ω-m along the southern margin of the NC where it meets the Uchi subprovince.

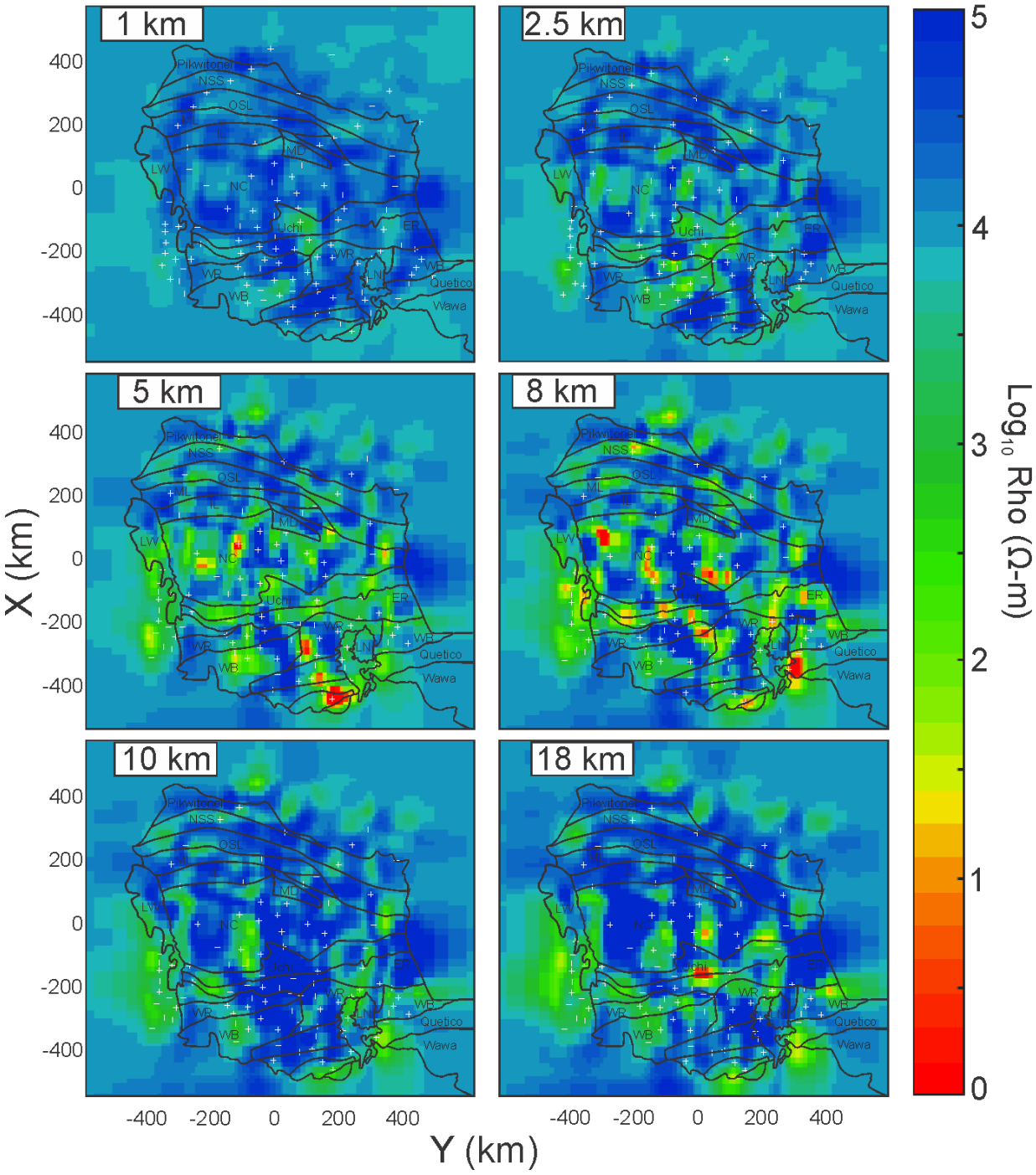

Figure 3: Depth slices through the first 18 km of the model. Crosses indicate site locations. Solid black lines indicate subprovince boundaries. NSS: northern Superior superterrane, OSL: Oxford-Stuff Lake terrane, ML: Munro Lake subprovince, IL: Island Lake subprovince, MK: Muskrat Dam subprovince, NC: North Caribou terrane, ER: English River subprovince, WR: Winnipeg River subprovince, WB: Wabigoon subprovince, LW: Lake Winnipeg, LN: Lake Nipigon.

The section of the model north of the NC terrane remains relatively unchanged between depths of 25 to 56 km, with resistivity values in general greater than 5000 Ω-m. At 25 km depth, the conductive regions of the model are constrained largely to the southern portions of the model, including the southern margin of the NC terrane. The central part of the NC, especially those regions near its southern margin, exhibit a significant decrease in resistivity between 38 and 56 km depth. The region of decreased resistivity terminates near the northern margin of the NC. A large, 200 km long and 60 km wide conductive region appears to the southwest of Lake Winnipeg at 26 km depth. This zone extends across the western margin of the NC, with a brief 50 km wide region of increased resistivity occurring beneath Lake Winnipeg itself. The same pattern is visible in the 38 km depth slice as well, with the notable difference that the conductive region no longer terminates just east of the margin, instead extending eastward into the interior of the NC. Likewise, conductors initially confined to the boundaries between the NC and Uchi subprovinces begin extending northward into the interior of the NC. By 56 km depth, the entire southern section as well as a significant portion of the central portion of the model are fairly conductive, except for a cross-shaped resistive anomaly centered near the north-south running boundary of the WB and WR subprovinces, to the west of Lake Nipigon.

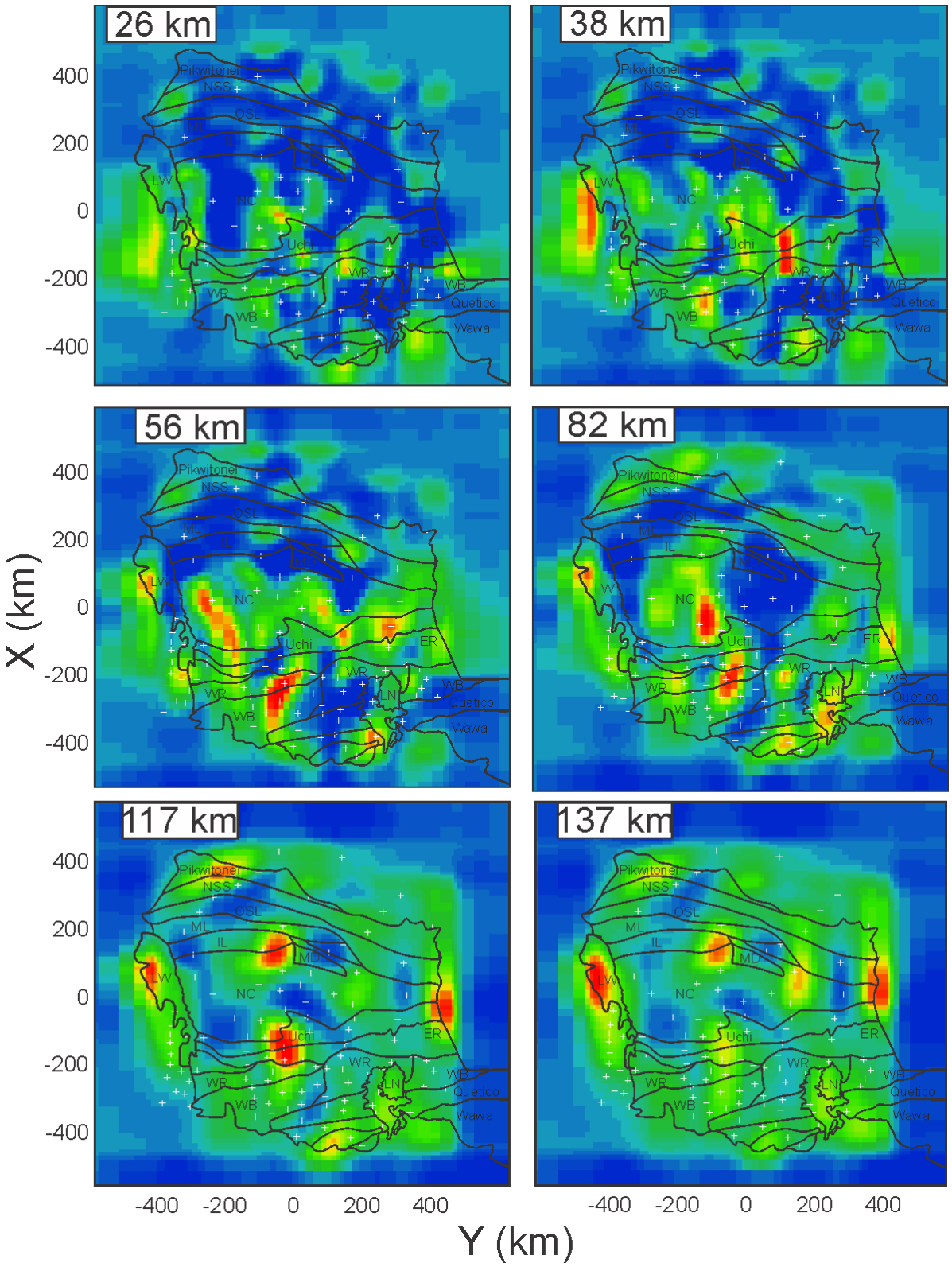

Figure 4: Depth slices between 26 km and 137 km.

The majority of the conductive features between 117 and 162 km depth are aligned roughly south-north. Within and north of NC, the majority of the conductors lie along subprovince boundaries. There are notable conductors along the east and west boundaries of NC, as well as long its northern margin. At 162 km depth, the interior of the NC is noticeably resistive compared to the rest of the model. There is a marked change in both the orientation and location of the conductors at 223 km depth. Conductive regions from the western and eastern edges of the model begin to join together within the interior of the NC, forming a 700 km long and 200 km wide feature at 308 km depth. It is worth noting that 30% of the sites do not have data at periods greater than 1000 s. In particular, none of the sites north of the NC have data above 1000 s.

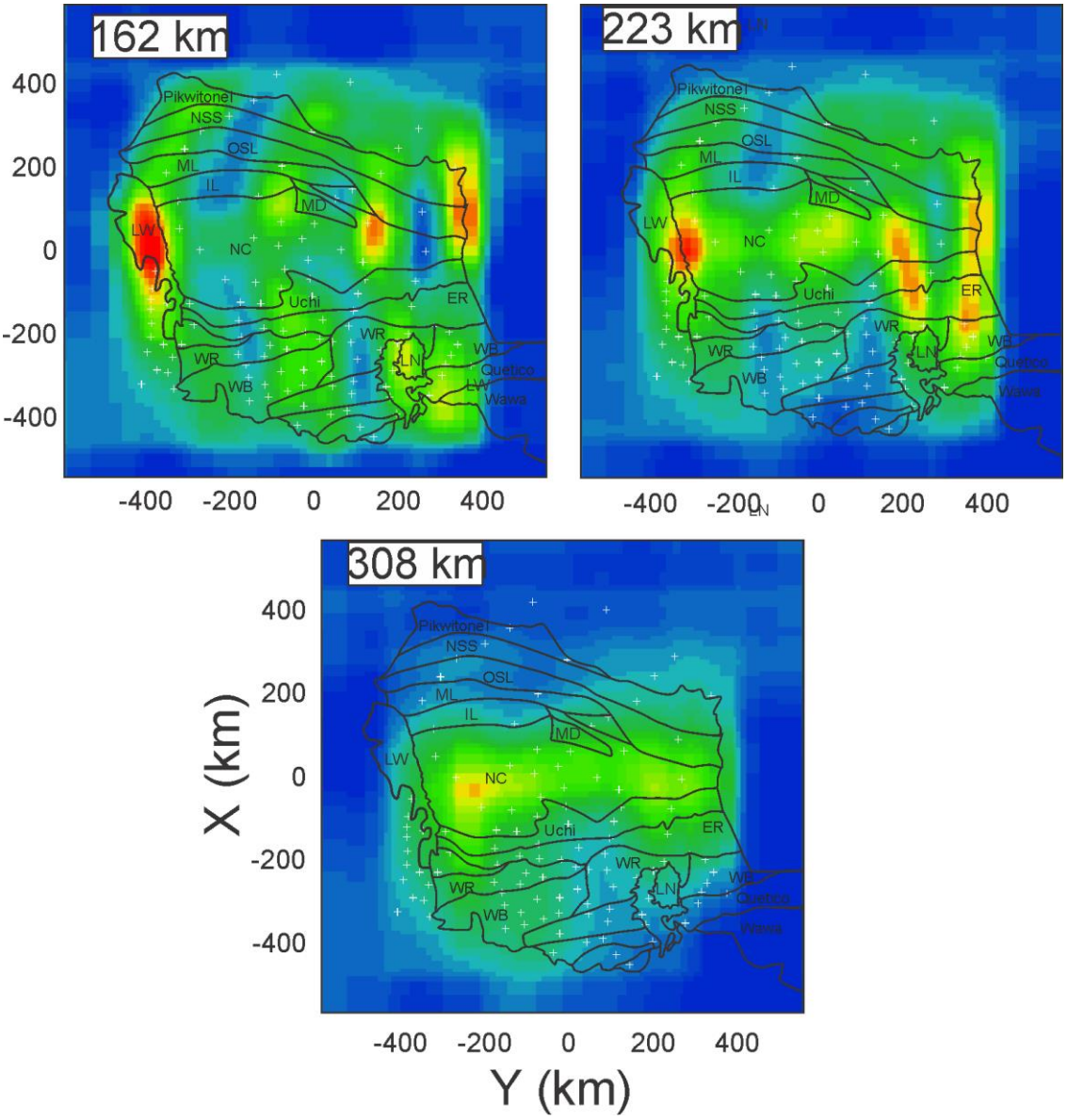

Figure 5: Depth slices between 162 km and 308 km.

Data Fit

The overall RMS of the final model is 2.28, which is reasonably low considering the model size and the number of data parameters. The RMS misfit of each of the inverted components is given in Table 1. The total misfit of the inverted components is between 1.6 and 2.9, with the highest values found at the imaginary parts of each impedance component. This trend is reversed for the tipper data, where the higher misfits are found at the real parts.

Table 1: RMS misfit for each data component.

Component	Base Error Multiplier	RMS Misfit
ZXXR	5	1.94
ZXXI	5	2.51
ZXYR	1	2.10
ZXYI	1	2.87
ZYXR	1	1.88
ZYXI	1	2.47
ZYYR	5	1.32
ZYYI	5	2.87
TZXR	1	2.66
TZXI	1	1.85
TZYR	1	2.66
TZYI	1	1.63

The RMS misfit of the data on a per-site basis is relatively uniform. Figure 6 shows the overall misfit at each site. The fit tends to be best for sites in the north of the model, although this is helped somewhat by the fact that many of these sites have dummy data and very high errors at the highest periods, which will tend to drive down the RMS. The sites with the worst fit are found in the south-central part of the model, including site 98-1_063, which has the highest overall RMS misfit at 5.9. This anomalously high misfit comes largely (although not entirely) from a poor match to the diagonal impedance components. Figures 7 shows data fit curves at 9 sites for the off-diagonal and diagonal components of the impedance tensor, respectively. In addition to analyzing individual components of the impedance tensor, it is often useful to consider apparent resistivities derived from the data. Rather than using the apparent resistivities at each impedance component, a single rotationally invariant 'determinant average' apparent resistivity is often used. These values are calculated using the mathematical determinant of the impedance tensor at each period (Figure 8). In general, the match

between the data and the model response are fairly good, even at sites with above average RMS. For instance, site 98-1_075 has good fit to both the diagonal and off diagonal impedance components, as well as to the tipper data (not shown). Nonetheless, the site's overall RMS is well above the average at 3.5. It is likely that the RMS values at some of the sites is inflated due to the relatively low errors used on the diagonal impedance components.

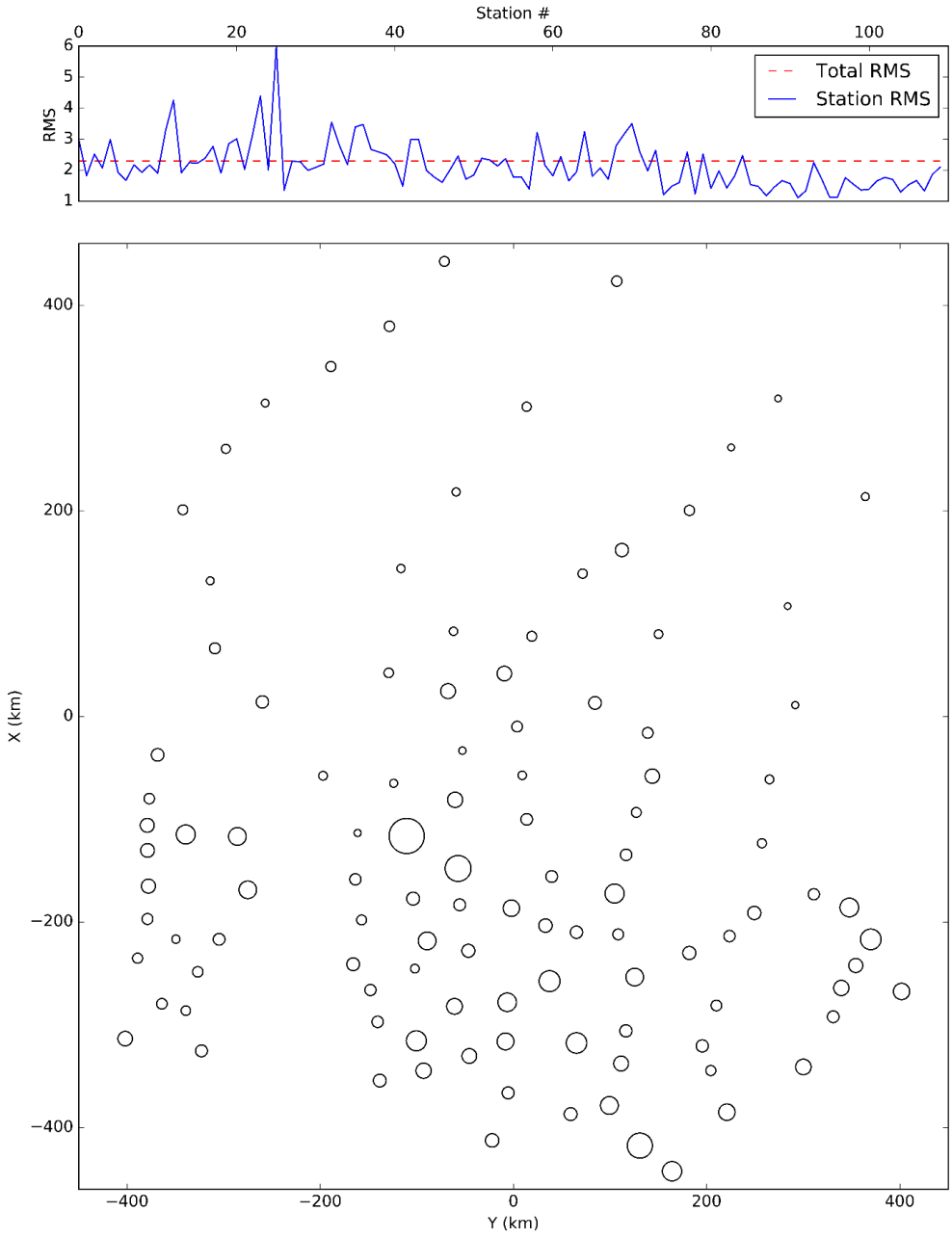

Figure 6: RMS misfit per station.

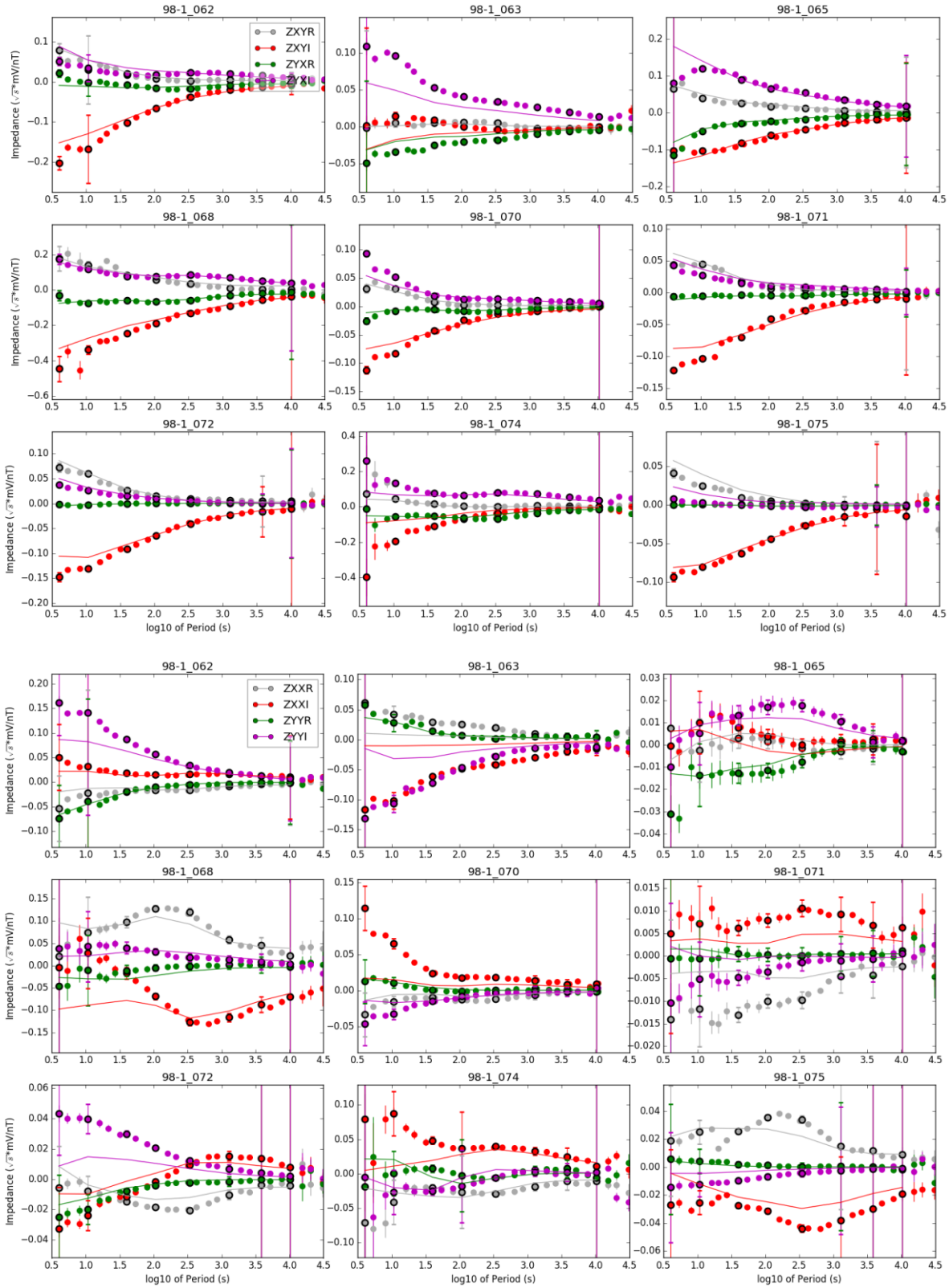

Figure 7: Data / model response plots for 9 sample stations. Black outlines indicate data points which were included in the inversion.

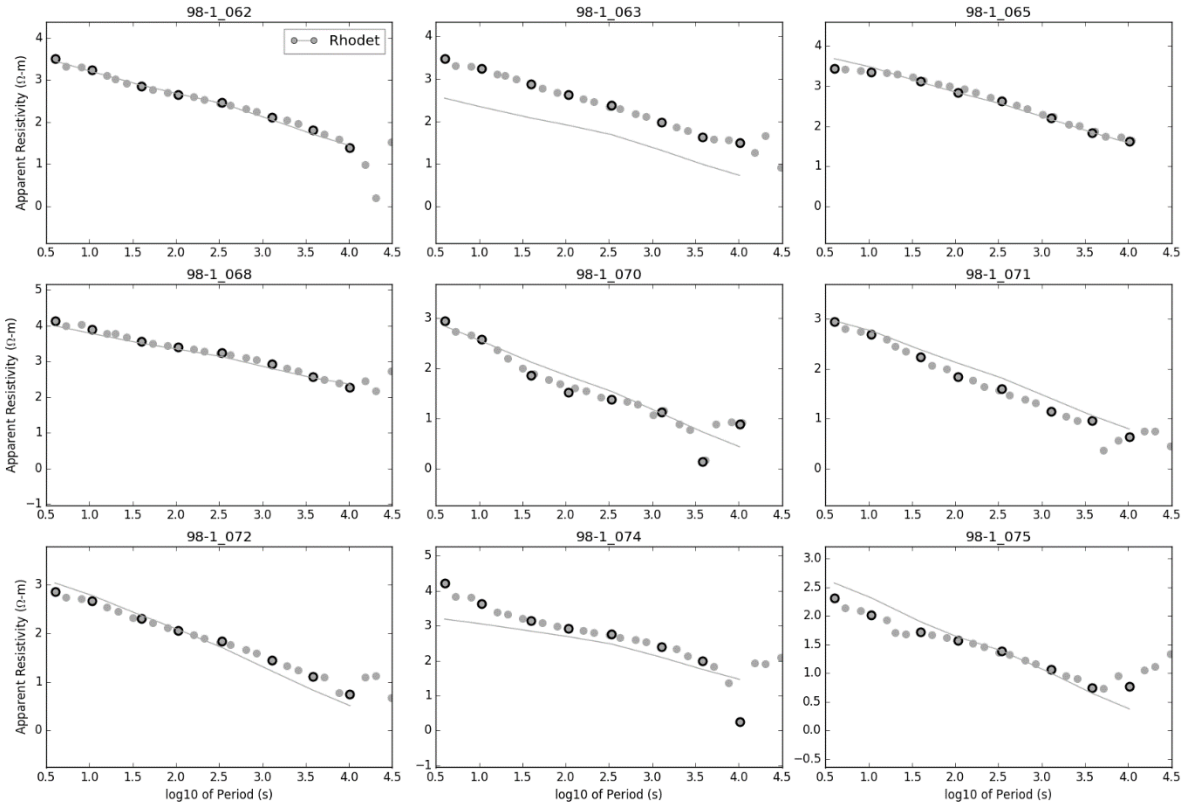

Figure 8: Determinant average data and model response plots for the same sites as shown in Figure 7.

Apparent Resistivity and Phase

The dataset collected across the Western Superior province has been previously inspected and interpreted by Ferguson et al., (2005). Primary MT responses calculated over the dataset were used to define first order geoelectrical structure in the region. Determinate average apparent resistivities and phases at short periods indicated a relatively resistive crust in the North Caribou terrane and a less resistive crust to the south. Long period responses suggested a relatively conductive upper mantle in the North Caribou, while that in the areas surrounding Lake Nipigon are relatively resistive. Ignoring sections shallower than 10 km depth, our model tends to agree with this assessment. Although some isolated conductors do exist in the NC terrane, it is largely resistive between depths of 10 to 30 km. The areas south of the NC, save for a region to the south-west of Lake Nipigon, are noticeably more conductive at these depths. The resistive feature surrounding Lake Nipigon persists until ~70 km depth, while at the same time the NC becomes considerably more conductive.

Figure 9 shows apparent resistivity contour maps generated using the raw data and the model response, as well as contour maps highlighting the differences between them, and Figure 10 shows

approximate depths for each period calculated using a Bostick-Niblett transform. The apparent resistivities calculated from the model responses match well with the data in most regions of the survey area. Apparent resistivities within and to the north of the NC match within half a degree of magnitude at both 4 s and 100 s, suggesting that these regions are largely resistive at crustal depths while becoming less resistive moving into the upper mantle, which agrees with both the past interpretations and with the model presented here. The apparent resistivities in the south-central part of the model response are over-estimated by nearly a whole order of magnitude at 4 s, which corresponds to a depth of ~30 km. The discrepancy is not as pronounced in the 100 s contour maps. A sensitivity test was performed by painting over the coincident area of the model coincident with a resistive zone. The overall RMS increased by 0.05, indicating that the decreased resistivity seen in the model at the southern margin of the NC at depths between 20 and 30 km depth is not supported by the data.

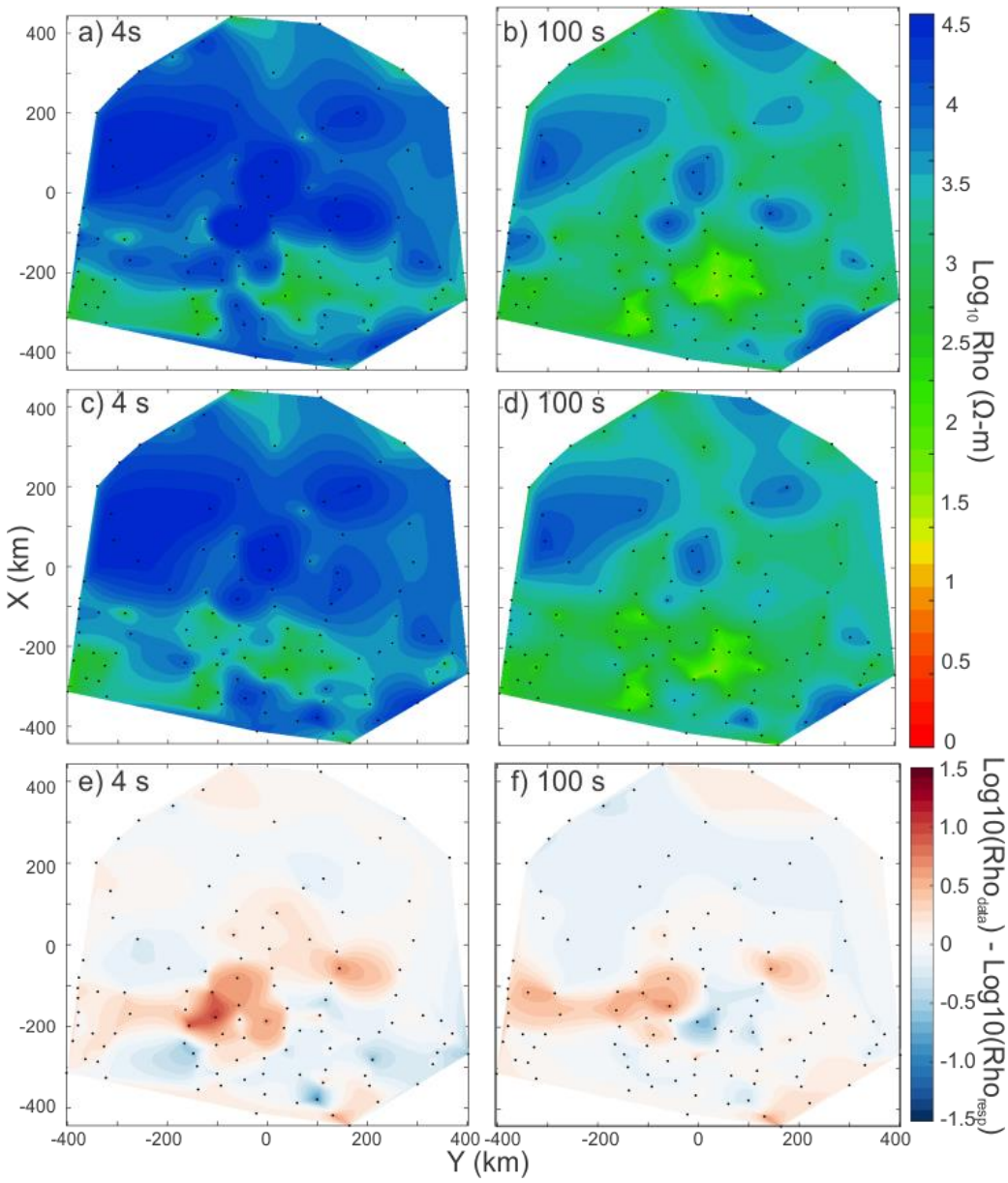

Figure 9: a) Determinant average apparent resistivity contour map calculated using the raw data at a period of 4 s and b) 100 s. c), d), as in a), b), but using the model response. e) Difference between log_{10} apparent resistivities calculated from the data and model response at 4 s and f) 100 s.

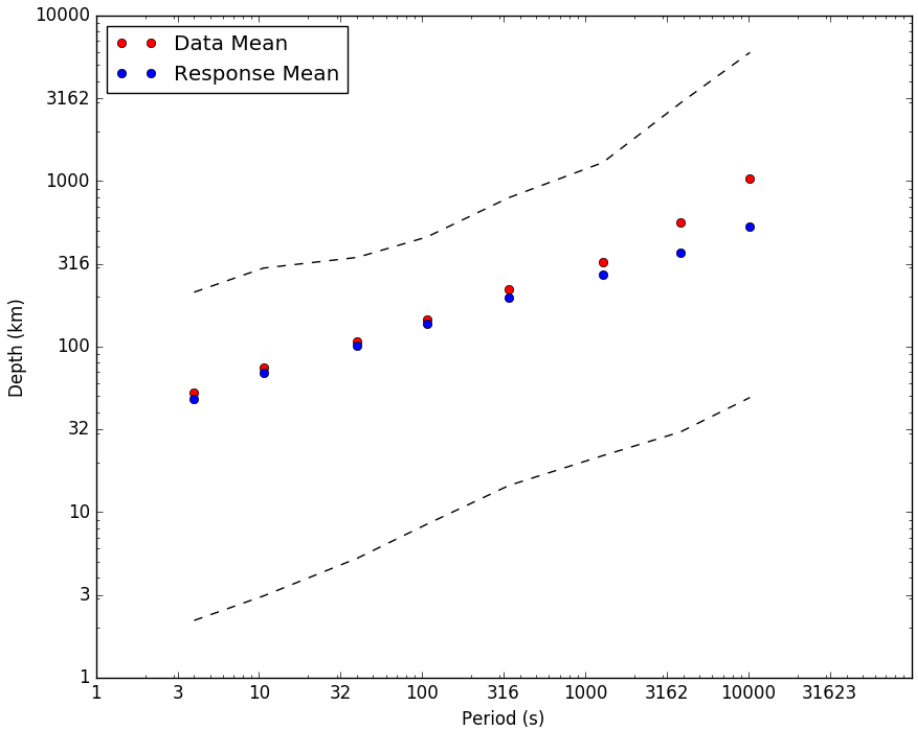

Figure 10: Average Bostick-Niblett depths for each period using in the inversion. Dashed lines indicate the minimum and maximum depths among all sites at each period.

Determinant average phase contour maps were also used during the initial interpretation of the data by Ferguson et al. (2005). Data and model response phase contour maps are given in Figure 11. At both 4 s and 100 s, the phase of the model response has an error of 6 degrees, on average. At 4 s, the error is significantly higher in the south of the model, with regions with phase differences as high as 20˚. At 100 s, the phase differences are typically less than 5˚ in the south, while the model response in the northwest section of the model has phases which are 10-20˚ higher than that of the data.

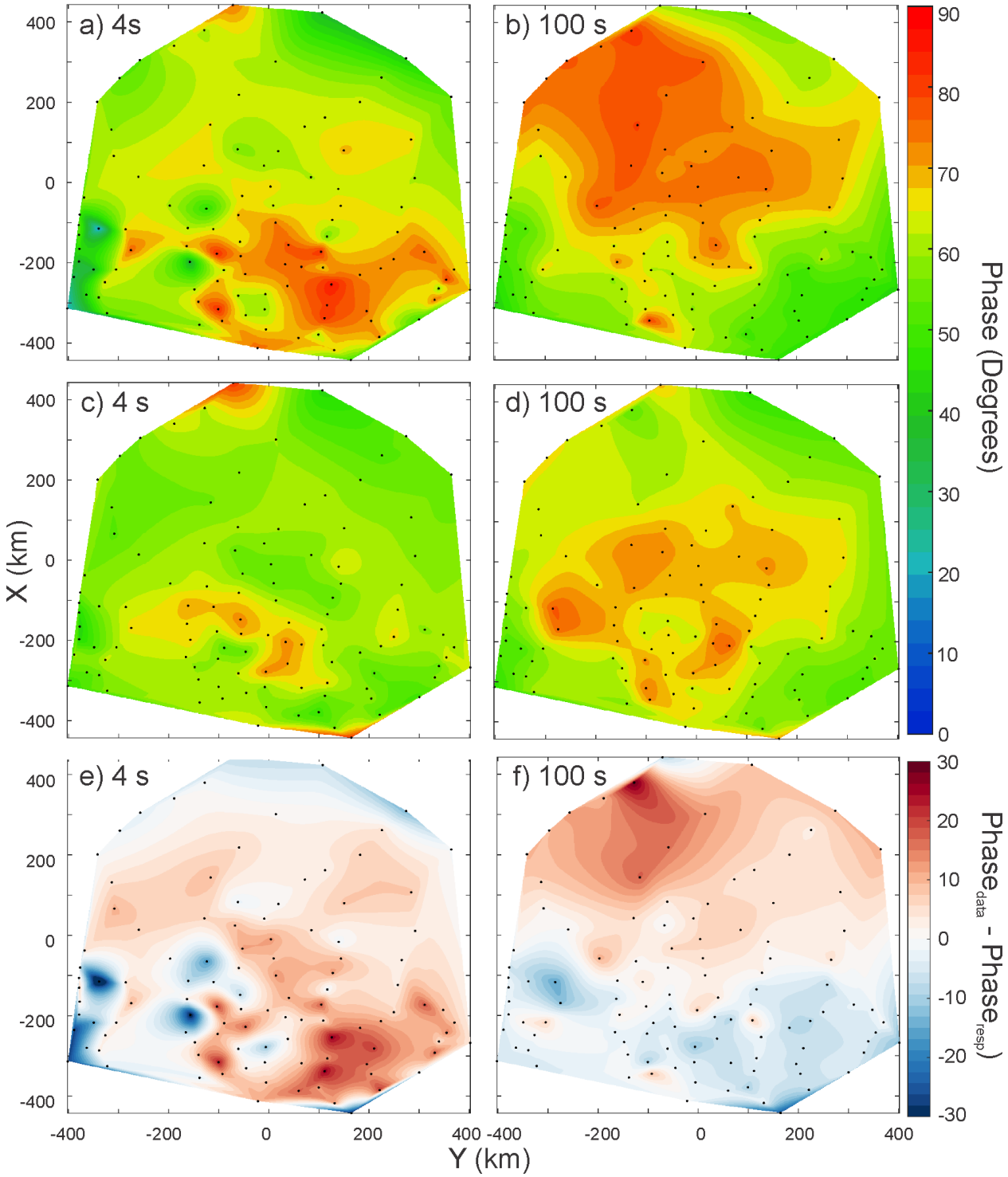

Figure 11: Determinant average phase contour maps of the data at a) 4s and b) 100 s. c), d) Same as a), b) but for the model response. e), f) Contour plots of a) – c) and b) – d), respectively.

Induction Arrows

In addition to the apparent resistivities and phases, Ferguson et al. (2005) also examined transfer function data collected over the Western Superior province. The transfer function can be represented graphically as 'induction arrows'. The Parkinson convention (Parkinson, 1962) of plotting induction arrows orients the real induction arrows such that they will tend to point towards more conductive regions. Figure 12 shows induction arrows plotting using the Parkinson convention as calculated using both the raw data and the model response at 4 and 100 s. The orientations of the arrows at 4 s are somewhat scattered for both the data and model response. The response arrows tend to match the data arrows more closely around the outsides of the model. There are likely local structures through the central parts of the model that are affecting that data but which were not resolved by the inversion. In contrast, the model response arrows at 100 s match quite well with the data in the interior of the model, while the data and response arrows in the north of the model tend to point in completely opposite directions. Figure 13 shows the induction arrows at 100 s plotted over a slice of the model at 138 km depth. While there is a conductive region to the northwest of the model, it is possible that the resistivity of this region of the model is higher than it should be and therefore does not elicit the same induction arrow response seen in the data. The apparent resistivity contour plots shown in Figure 9 support this, as Figure 9e) indicates that the apparent resistivities in the north of the model are slightly higher than the data would suggest. The arrows in the southern section of the model (below X = 0 km) match relatively well, however some trends seen in the data are not found in the model response. Ferguson et al. (2005) noted that there is a reversal in the north-south components of the induction arrows corresponding to the southern margin of the English River subprovince (given by the white dashed line in Figure 13). The model response induction arrows exhibit similar behavior in the central part of the model between -200 and 200 km in the west-east direction, however the arrows east of this tend to point southward towards conductive feature found at the southeast corner of the depth slice.

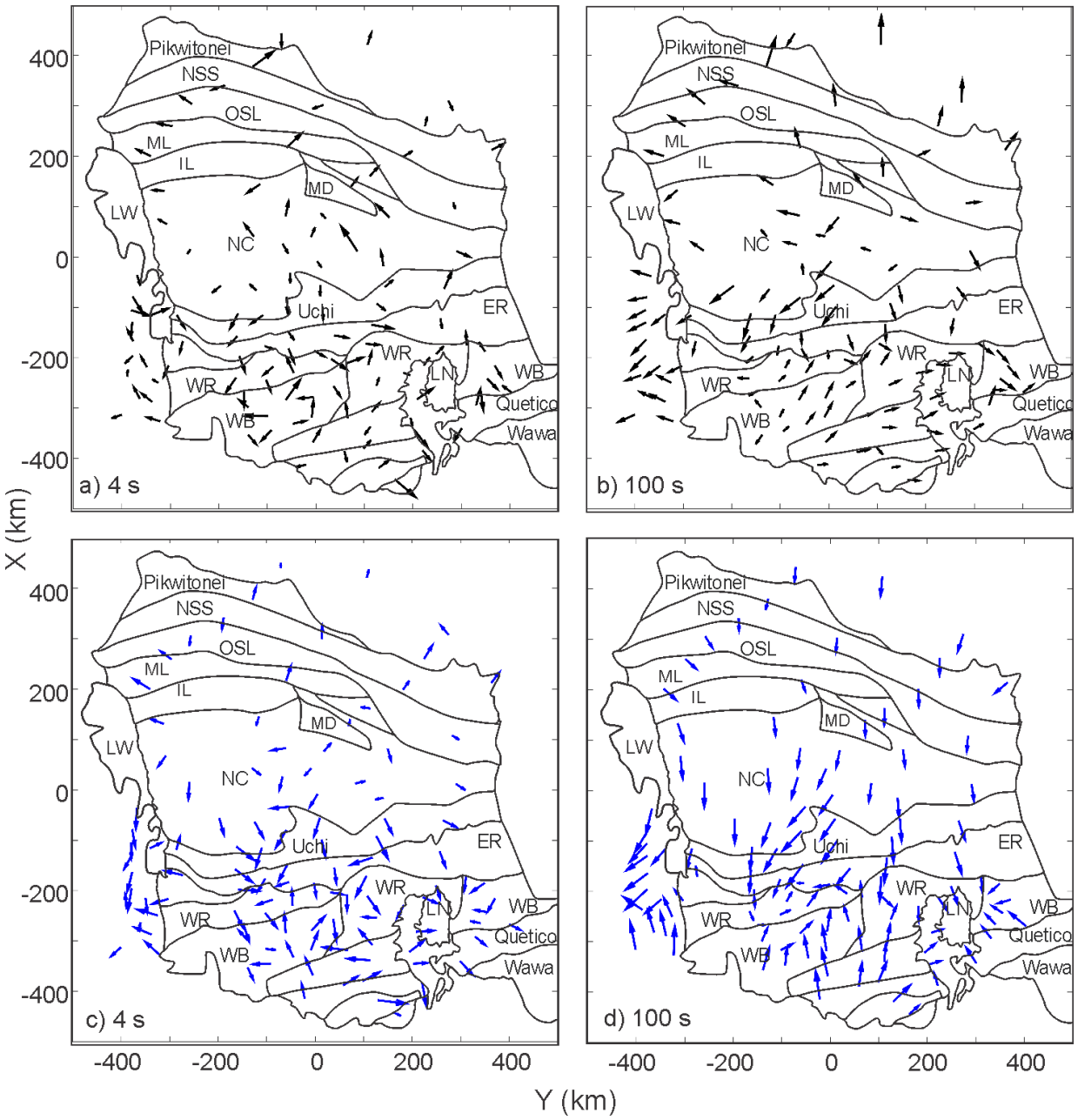

Figure 12: Induction arrow responses at a) 4 s and b) 100 s from the raw data. c), d) as in a), b), but using the model response.

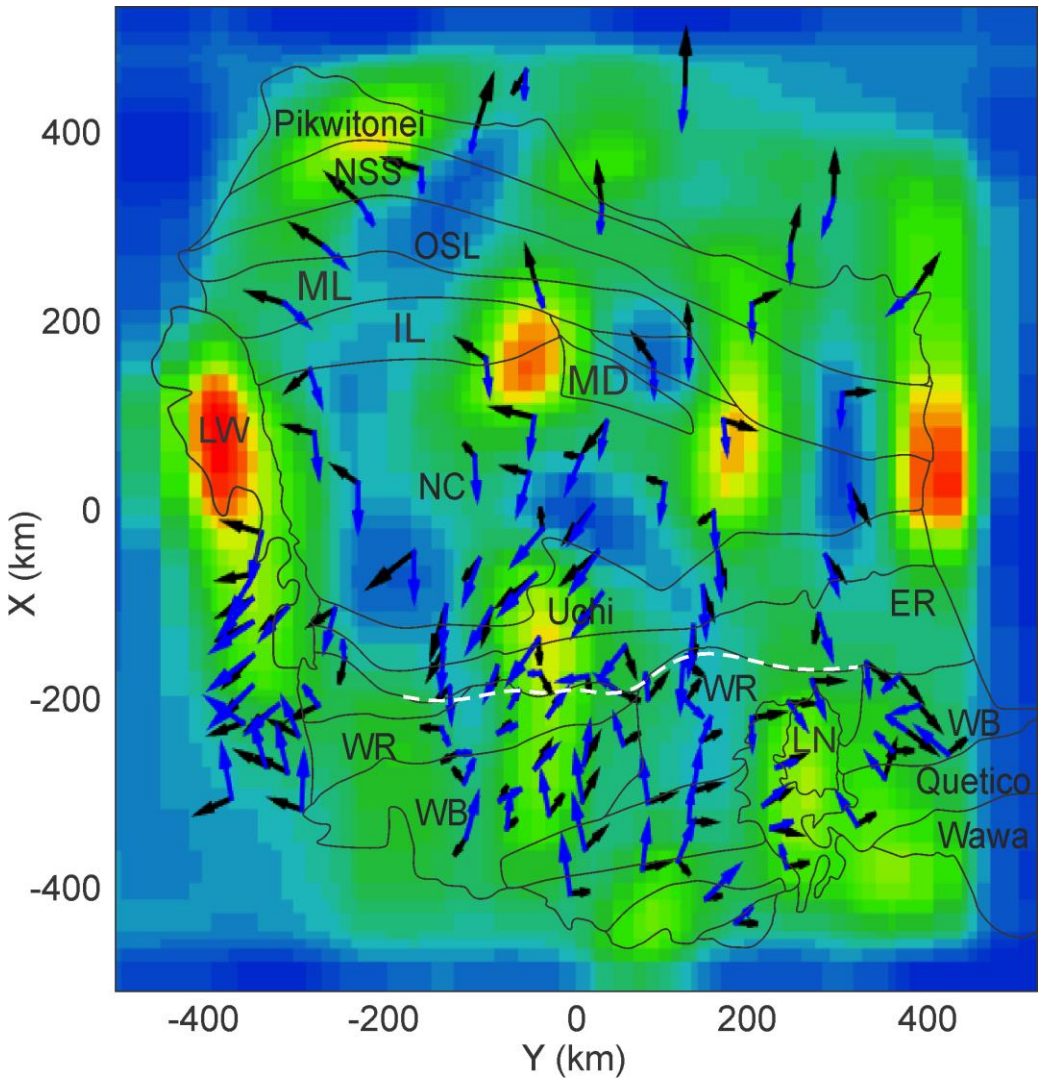

Figure 13: Data induction arrows (black) and model response induction arrows (blue) at 100 s plotted over a depth slice through the model at 138 km. The dashed white line represents the boundary of the data induction arrow reversal.

Discussion

Impedance and transfer function data was collected at 213 stations throughout the Western Superior province. Due to computational restrictions, it was impossible to invert the full dataset. Based on an analysis of spatial distribution of the data sensitivity at the lowest periods, 110 sites were selected for inversion. The final model resulting from inversion had an overall RMS misfit of 2.28. The stations in the north of the model tended to have lower than average RMS, while those in the south tended to have slightly higher RMS misfits.

The large scale features of the model largely agree with past interpretations of the dataset. Apparent resistivities at periods corresponding to crustal depths in the north of the survey area tended to be

higher than that in the south. This trend is also observed in the model. Both the model and the apparent resistivities suggest that the mantle lithosphere beneath the North Caribou terrane is relatively conductive. The same is generally true to the south of the NC, save for a prominent resistive feature found around and to the southwest of Lake Nipigon between ~26 km to 60 km depth.
Finer details of the structure of the Western Superior province are not as clear from the inversion results. Interpretations of the geoelectrical strike in past studies indicated that geoelectrical structures in the south of the survey area are aligned with the subprovincial boundaries, however there is very little structure in the model which corroborate this. Additionally, past analysis of the induction arrows suggested a 600 km long west-east trending conductive anomaly to the south of the English River subprovince (Ferguson et al., 2005). The model contains no clear structures which correlate with this such an anomaly.

There are a few features in the model which correlate with known structures. We start our discussion at depths of 137 km (Figure 14). The yellow outlines indicate the more prominent features in the model, which include a kidney shaped anomaly in the southeast corner which correlates spatially with the Nipigon Embayment previously identified from the data by Ferguson et al. (2005). This feature is clearly evident in tomographic P wave models for the region (Frederiksen et al. 2013). Most of the features are traceable to more shallow depths and the outlines have been reproduced in Figure 14 at depth slices where they are evident. Circular chimney-like conductors in MT models can be related to recent metasomatism during kimberlite ascension (e.g. Snyder et al. 2014; Adentuji et al, 2014). It is interesting to note the three conductors along the northern border of the North Caribou define a trend which can be extrapolated to the known kimberlites at Attawapiskat (see geology map in top left of Figure 14). At 82 km depth a prominent resistive feature (outlined in blue) with a broadly north-south trend is apparent. This feature is enigmatic but we note that Bedard and Harris (2014) suggest a north-south trend in Lu-Hf systematics (white dashed line in Figure 14) indicative of a proto Superior Province. Seismic studies (cf. Bedard and Harris, 2014) have also imaged regional north-south features in this region. At 56 km depth we note a broad moderately conductive region that contains within it two broadly north-south aligned highly conductive regions. This broad east west zone is perhaps responsible for the 2D behavior and induction arrow patterns of earlier studies as noted earlier, but the origin of the features remains enigmatic. Two further conductors with largely north-south orientation are apparent at the 38 km depth slice as well. Their interpretation remains speculative

as well at this juncture. We point out that a number of north-south features are apparent in gravity "worms" for the western Superior (Bedard and Harris, 2014), but have not done a direct comparison of our features with the worms at this time. More detailed work utilizing broader band (shallow penetrating) MT data is warranted. A prominent conductive region beneath and to the to southwest of Lake Winnipeg between depths of 38 and 137 km. While the data seems to suggest a conductive feature in the vicinity of Lake Winnipeg, the lack of data to the west and north of the anomaly means that its geometry and extent is poorly constrained.

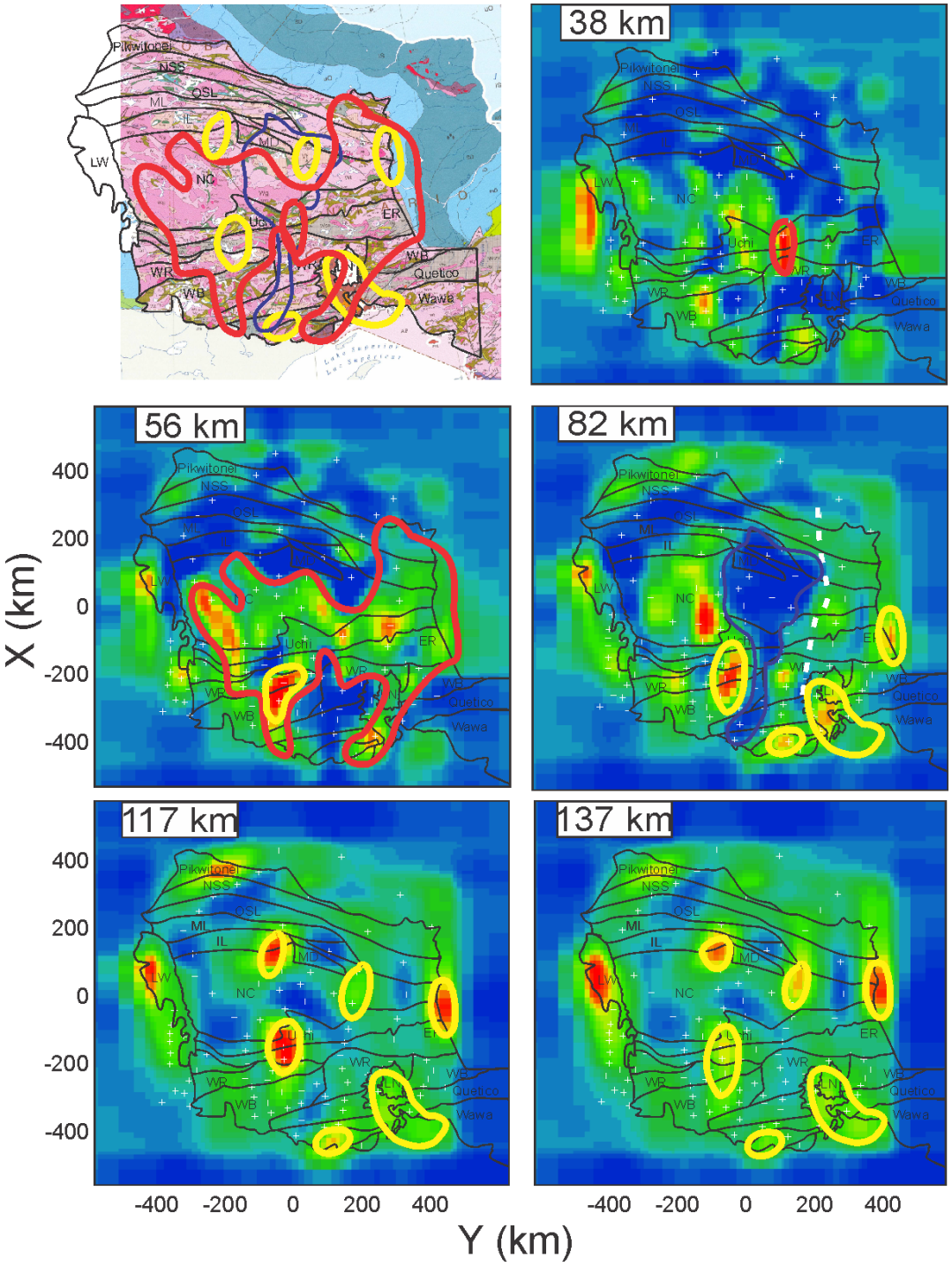

Figure 14 Outlines of major conductors from Figure 4 as discussed in text, and reproduced on a map of the geology in upper left.

Conclusions

While the model response matches fairly well to the data that was inverted, data from over half of the stations collected across the Western Superior province had to be excluded from inversion. The largest barrier to being able to invert the full Western Superior dataset, while allowing sufficiently fine model discretization, is the amount of memory required to store the sensitivity matrix. In order to better resolve geoelectrical structures from such large datasets, either more memory or an inversion algorithm which does not explicitly store the full sensitivity matrix are required. Alternately, overlapping focused inversions could be performed.

References

Adetunji, A.Q., Ferguson, I.J., Jones, A.G., 2014. Tectonophysics Crustal and lithospheric scale structures of the Precambrian Superior – Grenville margin. Tectonophysics 614, 146–169. doi:10.1016/j.tecto.2013.12.008

Bedard, J.H and Harris, L.B., 2014, Neoarchean disaggregation and reassembly of the Superior craton, Geology 42(11), 951–954, doi:10.1130/G35770.1

Bedrosian, P.A., 2016. Making it and breaking it in the Midwest: Continental assembly and rifting from modeling of EarthScope magnetotelluric data. Precambrian Research 278, 337–361. doi:10.1016/j.precamres.2016.03.009

Ferguson, I.J., Craven, J.A., Kurtz, R.D., Boerner, D.E., Bailey, R.C., Wu, X., Orellana, M.R., Spratt, J., Wennberg, G., Norton, M., 2005. Geoelectric response of Archean lithosphere in the western Superior Province, central Canada. Physics of the Earth and Planetary Interiors 150, 123–143. doi:10.1016/j.pepi.2004.08.025

Kiyan, D., Jones, A.G., Vozar, J., 2014. The inability of magnetotelluric off-diagonal impedance tensor elements to sense oblique conductors in three-dimensional inversion. Geophysical Journal International 196, 1351–1364. doi:10.1093/gji/ggt470

Parkinson, W.D., 1962. The influence of continents and oceans on geomagnetic variations. Geophysical Journal of the Royal Astronomical Society 6, 441–449.

Siripunvaraporn, W., Egbert, G., Lenbury, Y., Uyeshima, M., 2005. Three-dimensional magnetotelluric inversion: Data-space method. Physics of the Earth and Planetary Interiors 150, 3–14. doi:10.1016/j.pepi.2004.08.023